Technical Report Documentation Page

1. Report No.	2. Government Accession No.	3. Recipient's Catalog No.
2025GL118386		

4. Title and Subtitle	5. Report Date
Contrail observation limitations using geostationary satellites	November 2025
	6. Performing Organization Code

7. Author(s)	8. Performing Organization Report No.
Euchenhofer, M. V., Prashanth, P., Parke,S. A., Eastham, S. D., & Waitz, I. A.	

9. Performing Organization Name and Address	10. Work Unit No. (TRAIS)
Center of Excellence for: Alternative Jet Fuels and Environment Massachusetts Institute of Technology, Cambridge, MA, USA	11. Contract or Grant No. 13-C-AJFE-MIT-086

12. Sponsoring Agency Name and Address	13. Type of Report and Period Covered
Federal Aviation Administration Office of Environment and Energy	Journal Article
	14. Sponsoring Agency Code

15. Supplementary Notes

Euchenhofer, M. V., Prashanth, P., Parke, S. A., Eastham, S. D., & Waitz, I. A. (2025). Contrail observation limitations using geostationary satellites. Geophysical Research Letters, 52, e2025GL118386. https://doi.org/10.1029/2025GL118386

16. Abstract

Contrails are a significant contributor to aviation's climate impact with an effective radiative forcing similar to that from aviation's CO2 emissions, yet large uncertainties remain. Many observational contrail studies rely on data from a single sensor, in recent years increasingly from a geostationary imager, accepting lower spatial resolution in exchange for higher temporal and spatial coverage. However, the ability of geostationary imagery to resolve contrails has not been systematically characterized. By comparing higher spatial resolution low Earth orbit satellite imagery from Visual Infrared Imaging Radiometer Suite (VIIRS) to geostationary satellite imagery from GOES ABI, we show that the latter does not resolve 80% of the contrails nor half of the total length compared to contrails identified with VIIRS. Our findings underscore the need for multi-sensor approaches to collect observational contrail data for improved validation of climate models and to enable more rigorous and verifiable contrail avoidance strategies.

17. Key Words	18. Distribution Statement
ASCENT	

19. Security Classif. (of this report)	20. Security Classif. (of this page)	21. No. of Pages	22. Price
Unclassified	Unclassified		

Geophysical Research Letters

RESEARCH LETTER
10.1029/2025GL118386

Contrail Observation Limitations Using Geostationary Satellites

Marlene V. Euchenhofer[1], Prakash Prashanth[1], Sydney A. Parke[1], Sebastian D. Eastham[2], and Ian A. Waitz[1]

[1]Department of Aeronautics and Astronautics, Massachusetts Institute of Technology, Cambridge, MA, USA, [2]Department of Aeronautics, Imperial College London, London, UK

Key Points:

- Contrails are manually identified in false-color satellite imagery from a geostationary sensor and a sensor in low Earth orbit
- Differences in the number, cover, and the geometric features of the two observed contrail populations are analyzed and compared
- The study finds that geostationary imagers miss 80% of all contrails and half of their total length observed from low Earth orbit imagers

Supporting Information:

Supporting Information may be found in the online version of this article.

Correspondence to:

M. V. Euchenhofer,
euchmv@mit.edu

Citation:

Euchenhofer, M. V., Prashanth, P., Parke, S. A., Eastham, S. D., & Waitz, I. A. (2025). Contrail observation limitations using geostationary satellites. *Geophysical Research Letters*, *52*, e2025GL118386. https://doi.org/10.1029/2025GL118386

Received 22 JUL 2025
Accepted 26 NOV 2025

Author Contributions:

Conceptualization: Marlene V. Euchenhofer, Sebastian D. Eastham, Ian A. Waitz
Data curation: Marlene V. Euchenhofer, Sydney A. Parke
Formal analysis: Marlene V. Euchenhofer
Funding acquisition: Prakash Prashanth, Ian A. Waitz
Methodology: Marlene V. Euchenhofer
Project administration: Prakash Prashanth, Ian A. Waitz
Software: Marlene V. Euchenhofer
Supervision: Ian A. Waitz
Visualization: Marlene V. Euchenhofer, Prakash Prashanth
Writing – original draft: Marlene V. Euchenhofer

Abstract Contrails are a significant contributor to aviation's climate impact with an effective radiative forcing similar to that from aviation's CO_2 emissions, yet large uncertainties remain. Many observational contrail studies rely on data from a single sensor, in recent years increasingly from a geostationary imager, accepting lower spatial resolution in exchange for higher temporal and spatial coverage. However, the ability of geostationary imagery to resolve contrails has not been systematically characterized. By comparing higher spatial resolution low Earth orbit satellite imagery from Visual Infrared Imaging Radiometer Suite (VIIRS) to geostationary satellite imagery from GOES ABI, we show that the latter does not resolve 80% of the contrails nor half of the total length compared to contrails identified with VIIRS. Our findings underscore the need for multi-sensor approaches to collect observational contrail data for improved validation of climate models and to enable more rigorous and verifiable contrail avoidance strategies.

Plain Language Summary About half of aviation's climate impact is estimated to come from non-CO_2 effects, predominantly contrails, which are the line-shaped ice clouds that sometimes form behind airplanes. Many contrails can be avoided by small aircraft altitude adjustments to bypass the often thin layers of higher humidity in which they form and persist, making this an attractive opportunity for near-term climate impact mitigation. Since the ability to forecast the location of these thin regions in the upper atmosphere is limited, studies often rely on observations of contrails in imagery from geostationary satellites instead. However, the impacts of the limited spatial resolution of such geostationary images on contrail observations have not been rigorously assessed. In this study, we compare images taken from low Earth orbit satellites, which are higher in resolution, to those taken at the same time and location using a geostationary satellite. We find that the lower-resolution geostationary images miss 80% of the contrails observable with the higher-resolution instrument. These results have important implications for understanding contrail impacts and developing observation and forecasting systems for avoiding contrails. The results suggest that it will be necessary to combine information from multiple sensors to validate climate models and inform mitigation strategies.

1. Introduction

Condensation trails (contrails) are ice clouds that can form during the mixing of the hot, moist aircraft engine exhaust jet with the ambient atmosphere (Kärcher et al., 2015). If formed in ice-supersaturated air (Appleman, 1953; Jensen et al., 1998), contrails can persist for up to several hours (Gierens & Vázquez-Navarro, 2018), eventually spreading into contrail cirrus and becoming almost indistinguishable from natural cirrus clouds (Haywood et al., 2009; Schumann, 1996). By interacting with incoming shortwave solar radiation and outgoing terrestrial longwave radiation, contrails affect the radiative balance of the atmosphere. While an individual contrail can be net warming, as is the case for all nighttime contrails (Meerkötter et al., 1999), or net cooling, on average contrails have a warming impact on the planet (Bock & Burkhardt, 2016; Burkhardt et al., 2010; Burkhardt & Kärcher, 2011; Chen & Gettelman, 2013; Kärcher, 2018; Meerkötter et al., 1999; Teoh et al., 2024). A recent meta-study estimates that contrails account for approximately half of aviation's effective radiative forcing (ERF) (Lee et al., 2021). However, most estimates of contrail climate impact and contrail cover are based on modeling simulations, with few observations to validate the projections, leading to high uncertainties (Bier & Burkhardt, 2022; Lee et al., 2021; Sanz-Morère et al., 2020). Notwithstanding these uncertainties, it is understood that contrail climate impacts can be significantly reduced if the regions that support contrail persistence are known and operationally avoided. The concept of contrail avoidance leverages the fact that ice-supersaturated layers generally are limited to a few hundred meters in altitude. Flights can be vertically deviated to avoid

Writing – review & editing: Marlene V. Euchenhofer, Prakash Prashanth, Sebastian D. Eastham, Ian A. Waitz

these regions and therefore mitigate the formation of persistent contrails and their associated radiative impacts (Teoh et al., 2020).

Satellite-based observations of contrails can provide critical insight for both climate modeling and operational avoidance. Specific use cases include the assessment of contrail climate impacts, the evaluation of model predictions of an individual contrail's extent and evolution, and the assessment of model predictions of humidity, as well as the identification of regions for operational contrail avoidance and the retrospective assessment of contrail formation for monitoring, reporting, and verification (MRV).

While some early investigations of contrails relied on ground-based observations from humans (Minnis et al., 1997, 2003) and more recently from ground-based cameras (Low et al., 2025; Mannstein et al., 2010; Schumann et al., 2013), most observational studies have applied satellite-based remote sensing to determine contrail cover, derive estimates of physical parameters and radiative forcing, and identify regions where contrails not only form, but also persist for several hours. Many satellite-based studies automated their contrail detection using line filters to identify linear contrails (Mannstein et al., 1999) or used specially trained convolutional neural networks to identify contrail pixels (Kulik, 2019; Meijer et al., 2022). Most of the earlier contrail investigations applied these approaches to data collected from polar-orbiting satellites in the low Earth orbit (LEO) (Bakan et al., 1994; Bedka et al., 2013; Duda et al., 2004, 2013, 2019; Mannstein et al., 1999; Meyer et al., 2002; Minnis et al., 2005, 2013; Palikonda et al., 2005), whereas in more recent years, there has been a shift toward leveraging data from geostationary (GEO) platforms (Chevallier et al., 2023; Geraedts et al., 2024; Kulik, 2019; Meijer et al., 2022; Ng et al., 2023; Vázquez-Navarro et al., 2015; Wang et al., 2022). Instruments onboard GEO platforms, including the Geostationary Operational Environmental Satellite (GOES) series, enable sustained large-scale assessments due to their near-hemispherical spatial coverage and continuous temporal sampling (every 5–10 min), contributing to their appeal over LEO data, especially for real-time identification of regions for operational contrail avoidance. The successful implementation of contrail avoidance relies on identifying three-dimensional regions where conditions support contrail persistence. Since weather forecast-based approaches cannot reliably resolve the upper atmospheric humidity to the level required (Agarwal et al., 2022; Gierens et al., 2020), avoidance regions are often estimated based on the widely available real-time observations of contrails from geostationary satellite data combined with altitude information from flight attribution (Chevallier et al., 2023; Gierens et al., 2020; Sonabend-W et al., 2024).

However, previous investigations have shown that observations from geostationary platforms do not sufficiently capture the occurrence of optically thin or geometrically narrow contrails due to the coarser resolution of the instruments. Contrail lifetime analysis from automated contrail detections showed that, due to limited instrument sensitivities, the total lifetime from initial formation to dissipation is expected to be up to three times greater than that observed from an infrared instrument onboard a geostationary satellite (Gierens & Vázquez-Navarro, 2018). Simulations of the appearance of linear contrails over clear sky with an ocean background in satellite imagery, similar in resolution to that of the GOES Advanced Baseline Imager (ABI), indicate that such instruments can resolve less than half of the modeled contrail population, in this “best-case observability” scenario (Driver et al., 2024). These two studies imply additional downstream effects on contrail MRV. The implications for identifying ice-supersaturated contrail avoidance regions are less straightforward.

Some studies have combined data from GEO and LEO satellites (Duda et al., 2004; Minnis et al., 2008, 2013; Vazquez-Navarro et al., 2010; Vázquez-Navarro et al., 2015). Others have simulated contrail occurrence to quantify contrail cover and compare it to observational estimates (Kärcher et al., 2009) or to model the observational capabilities of different satellite imagers in capturing contrails (Driver et al., 2024). However, to our knowledge, no study to date has systematically compared observations of a set of identical scenes in time and location across different remote sensing instruments and tied the findings to the range of use cases mentioned earlier. In this work, we present contrail observations from two different imagers, ABI (2–3 km resolution) and the Visual Infrared Imaging Radiometer Suite (VIIRS; 750 m resolution) that, for the first time, enable a large-scale comparison between contrails in GEO and LEO satellite imagery. We address the shortcomings in previous observational studies and derived contrail impact modeling by investigating the limitations in contrail observability of the ABI instrument. Our data set contains 1,667 and 7,731 individual contrail objects in ABI and VIIRS false-color imagery, respectively, manually identified in 12 distinct scenes, which are evaluated for total cover, effective width, and length distributions.

2. Data and Methods

2.1. Data Set and Images

Our data set consists of 12 scenes over the contiguous United States, varying in coverage between 1,273,152 km^2 and 7,196,251 km^2. One scene from each month in the period of December 2023 to November 2024 is included. See Table S1 in Supporting Information S1 for an overview. Scene selection was based on the availability of a VIIRS swath with significant overlap with the GOES CONUS (contiguous United States) region, while seeking to represent a range of scenarios for cloud cover, cloud types, and their co-occurrence with contrails. For each scene, a VIIRS NASA data product, provided on a regular latitude-longitude grid, from one of the three polar-orbiting satellites NOAA-20, NOAA-21, or Suomi NPP was accessed. The resulting spatial resolution of these projected images is about 500 m. For GOES-16 ABI, data from the five-minute time step closest to the time assigned to the VIIRS image were taken and reprojected onto a regular grid of 0.2° by 0.2°. False-color ash images were generated and stored as GeoTIFF rasters with EPSG:4326 as their coordinate reference system. The ash composite uses brightness temperatures and brightness temperature differences in the infrared spectrum to highlight both contrails and natural cirrus in dark blue (Meijer, 2024), a characteristic which, alongside their generally linear appearance, allows us to identify contrails in the imagery. These properties were leveraged by two trained individuals to label all visible contrails in the 24 images in the data set—one from GOES ABI and one from VIIRS for each of the 12 scenes—using the open source geographic information system QGIS (Quantum geographic information system). In the software, the data are displayed in full resolution in the equidistant cylindrical Platte Carrée projection. A displacement between the same contrail observed with the two different imagers stems from parallax (due to differing viewing geometries) and advection (the images were taken up to 2 min apart).

2.2. Contrail Objects

Labels were created directly as shapefiles in QGIS to preserve spatial information and store each label as a polygon object, thus allowing for an individual investigation of the properties of each contrail on its own. The number and lengths of the contrails were derived from the individual objects. The length of a contrail segment was approximated as the length of the centerline of the longer side of a minimum rotated bounding box around the polygon object with the total contrail length within each image comprising the sum of the lengths of all contrails labeled in the image. The effective width, as previously introduced in other studies (Vázquez-Navarro et al., 2015), is defined as the quotient of the area of the polygon and its length. The contrail area cover within one scene was retrieved from a binary mask in the native image's resolution that highlights all contrail pixels in the image rather than from the sum of the individual polygon areas to avoid double-counting of overlapping contrails.

2.3. Contrail Downsampling

For the downsampling analysis, each VIIRS contrail was coarsened such that its downsampled outline aligns with the ABI image grid. To obtain an upper-bound for the increase in contrail width, all pixels on the ABI grid intersected by the overlaid VIIRS contrail were considered to constitute the respective downsampled contrail. The effect on the contrail length was neglected such that the resulting effective width was calculated from the downsampled contrail area divided by the original contrail length. The downsampling factor is defined as the ratio between the width or cover of the downsampled contrail and its respective original value.

3. Results

3.1. Number of Observed Contrails

Contrail labels on ABI and VIIRS imagery for one of the investigated scenes are shown in Figure 1a. (See all scenes in Supporting Information S1, Section 1). We find that there are two types of ABI omissions: individual contrails missed in a cluster of identifiable contrails (Inset 1) and missed clusters (Inset 2).

We find that on average, across all scenes studied here, 20% of individually identifiable contrails as manually labeled in VIIRS images are observed with ABI. However, in Figure 1b we see that this percentage varies substantially across different scenes, ranging from 6.6% to 34.3%.

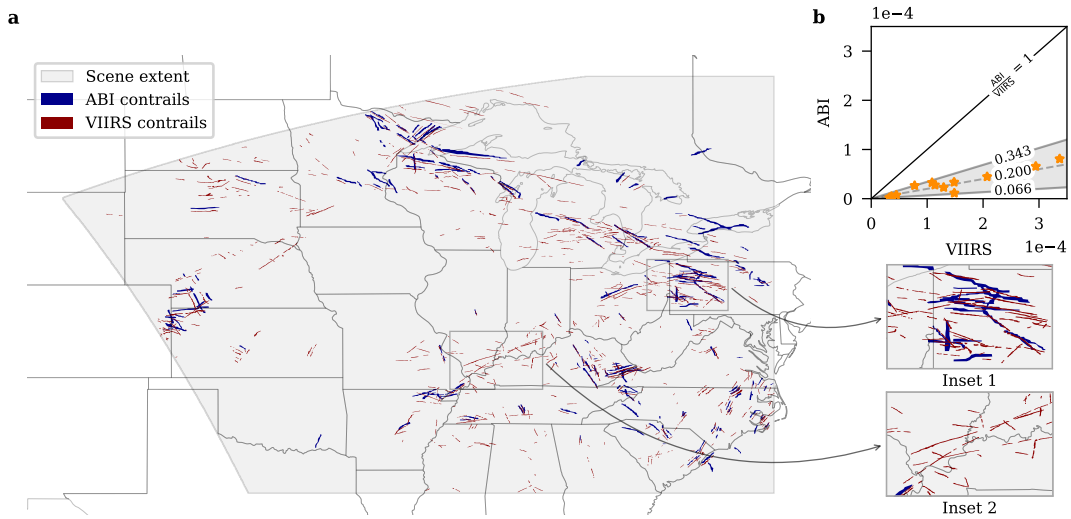

Figure 1. Contrails identified from both ABI (blue) and VIIRS (red) imagery on top of map showing scene extent for the scene on display. Insets show exemplary cases in which ABI misses contrails that are identified using VIIRS (a). Parity plot with contrail density in $\left[\frac{1}{\text{km}^2}\right]$ as observed with ABI and VIIRS, respectively, for all 12 scenes. Shaded area represents min-max range of $\frac{\text{ABI}}{\text{VIIRS}}$-ratio for those scenes. The average ratio for the whole data set is represented by the dashed gray line (b).

3.2. Observed Contrail Length

In two-thirds of the scenes, ABI resolves less than half of the total contrail length that is observable with VIIRS. For the individual scenes, the estimated total contrail length from ABI images ranges between 20.7% and 66.4% of the total contrail length derived from VIIRS with an average of 42% when considering the full data set (see Figure S13a in Supporting Information S1 for distribution).

To explain why the number of contrails missed by ABI compared to VIIRS is greater than the missed total contrail length, we examine the individual contrail lengths that contribute to the aggregated value. The respective distributions for ABI and VIIRS are presented in Figure 2a. Half of the contrails observed with ABI have estimated lengths between 30 and 70 km with the number of observations gradually decreasing for longer contrails, and only four observations falling into the category of shorter than 10 km. This distribution differs notably from the one obtained for VIIRS for which more than half of all visible contrails are between 10 and 30 km long. The number of observations decreases with increasing length, while VIIRS resolves more contrails in each length partition compared to ABI. However, the relative difference between the two diminishes with increasing contrail length. Under the assumption that most contrails identified with ABI are a subset of those identified with VIIRS, this implies that ABI tends to miss more shorter contrails than longer ones. This is particularly striking for contrails

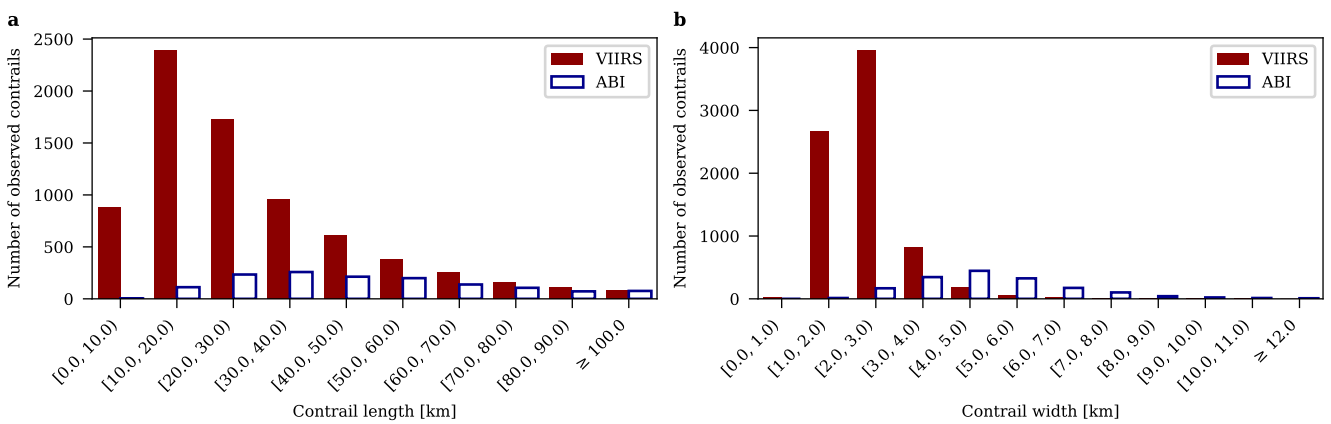

Figure 2. Absolute frequency of occurrence of observed contrail lengths (a) and widths (b) in VIIRS (dark red) and ABI (white with blue edge) imagery for all contrails in all scenes.

measuring less than 10 km, a population that makes up 10% of all VIIRS contrails in the data set. These shorter contrails are more prone to being missed by ABI, thus, while contributing less to the lower observed total length, reduce the ratio of the number of contrails observable from ABI.

3.3. Contrail Width and Cover

Figure 2b shows the number of observations in different effective width bins for all contrails identified from ABI and VIIRS imagery, respectively. While the ABI distribution is concentrated around its peak between 4 and 5 km with a decrease in either direction, 85% of all VIIRS contrails appear with widths below 3 km. Most notably, a third of all VIIRS contrails have an effective width between 1 and 2 km, a population that is not only negligible for ABI, but also lies below the instrument's minimum resolution and thus its practical limit for resolvable features.

Due to the generally high aspect ratio of contrails, resolution has a smaller effect on accurately resolving the length of a visible contrail, whereas the impact on the widths of the contrail observations is measurable. Certain narrow contrails do not meet the threshold to be resolved by the instrument and thus do not appear in the resulting image. However, some contrails that are observable can appear smeared due to undersampling, such that inaccurate width and area cover estimates are derived. We can see this by comparing the subgroups of wider contrails between ABI and VIIRS in Figure 2b. Unlike for the length distribution in Figure 2a, the number of ABI observations exceeds the number of VIIRS contrails within certain categories, namely, for contrails with an effective width above 4 km. Leveraging the previous assumption that the contrails observed with ABI are a subset of those identified using VIIRS, the higher frequency of wider contrails observed in imagery from ABI compared to VIIRS suggests that the lower resolution of ABI results in contrails appearing wider. This “blurring effect” results in an overestimate of the width and thus area of an individual contrail and has been pointed out previously for both natural cloud patterns (Shenk & Salomonson, 1972) and contrails (Driver et al., 2024).

The two identified factors, reduced number of contrail observations and increased observed width for certain observations, result in counteracting effects on the contrail area cover derived from ABI observations. Unlike for the underestimation in the number and the total length of contrail observations, we see more variation among the scenes. Considering all 12 scenes, the ABI-based estimate varies between 39.2% and 145.2% of the contrail cover identified using VIIRS. In five out of the 12 scenes, the contrail cover in the ABI imagery exceeds the cover observed with VIIRS (see Figure S13b in Supporting Information S1 for distribution of observed contrail cover). These five scenes correspond with those with the highest fractions of total contrail length observed with ABI relative to VIIRS.

3.4. Cover Overestimation

Contrail modeling and subsequent forcing estimates require accurate observational data for model validation, limitations to which we have pointed out (Burkhardt et al., 2010; Marquart et al., 2003; Meyer et al., 2002; Sanz-Morère et al., 2020). We quantify the “blurring effect” we observe for lower-resolution ABI imagery on observed contrail widths and cover by downsampling all contrails observed in VIIRS images to the resolution of the respective ABI images. The inset in Figure 3b visualizes the downsampling approach described in Section 2.3 with the dark red polygon showing an exemplary VIIRS contrail and the light red feature below representing the respective downsampled polygon on the coarser ABI image grid. This framework provides an upper bound to quantify the impact of lower-resolution on contrail cover overestimates. Since the respective length and width distributions in Figure 2 show that the differing resolutions only marginally affect the observed length, we assume the effect on the contrail length to be negligible and focus on the ABI overestimate of contrail width, which in turn drives the effect on the observed contrail area cover.

Figure 3a illustrates the distribution of effective contrail widths for the three subgroups of contrails: observed with ABI, observed with VIIRS, and VIIRS downsampled to the ABI resolution. The mean effective contrail width, represented by the horizontal black bars, differs between VIIRS (2.35 km) and ABI (4.94 km) by a factor of 2.1. The resulting average for the downsampled VIIRS contrails (5.33 km) exceeds the value for ABI by 8%, showing that our approach leads to a reasonable approximation for the average “blurring” effect. Before (after) downsampling the VIIRS contrails, 97% (96%) of contrails lie within a range of approximately ±2 km from the respective average width. 96% of the downsampled VIIRS contrail widths are greater than 4 km while we identify contrails with widths as small as 2 km with ABI. This discrepancy stems from our upper-bound approach, which accounts for all intersected grid cells being considered covered. Since the minimum width of an ABI pixel is about

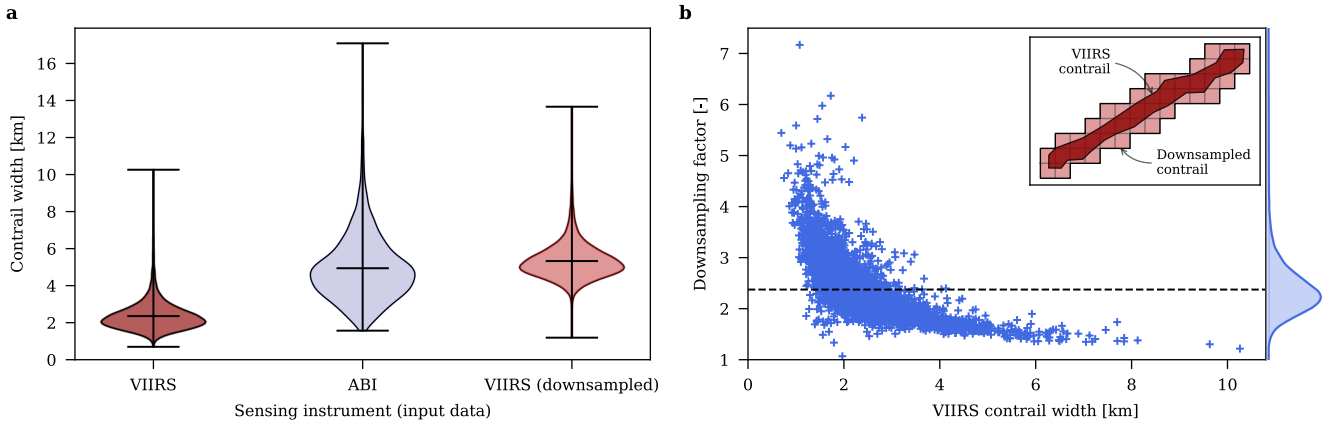

Figure 3. Violin plot with the distributions of effective contrail widths for all VIIRS (dark red), ABI (blue), and downsampled VIIRS (light red) contrails. The center black horizontal line in each violin represents the average contrail width for the respective subgroup (a). Distribution of downsampling factor, which describes the width (cover) ratio between the downsampled and the original VIIRS contrail, versus originally observed contrail width. The average is indicated by the dashed black line. A density distribution of the downsampling factor is given on the right *y*-axis. The inset further shows an example of the outline of a VIIRS contrail (dark red) and the pixels of its downsampled counterpart (light red) (b).

2 km, a VIIRS contrail has to lie exactly within the bounds of a row or column of pixels to be less than 4 km wide after downsampling.

We further introduce the downsampling factor, the ratio between downsampled and original contrail width, to quantify the effect of downsampling a VIIRS contrail on its width, and thus individual cover. Figure 3b reveals an inverse correlation between original contrail width and the downsampling factor. All contrails experiencing a downsampling factor greater than the mean (2.37 as indicated by the dashed black line) are less than 4.13 km wide, implying amplified blurring for narrower contrails. The density distribution on the right implies that 91% of VIIRS contrails experience a downsampling factor between 1.5 and 3.

If all contrails observed with VIIRS were also visible in ABI imagery, the contrail cover derived from ABI could be more than twice as large as that derived from VIIRS. Since we have shown that ABI resolves fewer contrails than VIIRS (see Figure 1b) and that wider contrails experience weaker blurring (see Figures 2b and 3b), we confirm our assumption that ABI is more likely to miss narrower contrails.

4. Conclusion and Discussion

Our scene-aggregated analysis for the number, total length, and observed cover of contrails shows that on average ABI misses about 50% of the total length and 80% of all contrails that can be observed using data from the higher-resolution instrument VIIRS in the same region and at approximately the same time. This fraction of unobserved contrails exceeds the estimates modeled by Driver et al. (2024), while this study derived a best-case estimate, thus providing a lower bound. The limitations in the contrail observation performance of geostationary satellite imagery affect both their utility to evaluate climate forcing models and to identify avoidance regions for operational contrail mitigation, with the latter also relying on the observed total contrail length as a measure to evaluate the effectiveness of avoidance trials (Sonabend-W et al., 2024).

An analysis of the geometric properties of the individual contrails, such as their individual lengths and effective widths, reveals that lower-resolution imagery fails to resolve both shorter and narrower contrails. The latter, in many instances, fall below the physical observability threshold that is given by the instrument's minimum pixel size, limiting the applicability of GEO observations for assessing model predictions of the extent of individual contrails. The missed shorter contrails can either be non-persistent and thus of negligible radiative impact, may grow enough to eventually become identifiable in subsequent frames from GEO satellites, or may be persistent and yet remain unobserved by geostationary imagers. Model-based contrail forcing analyses suggest that more aged and wider contrails, which, as we showed, are more frequently observed with ABI, contribute disproportionately to the overall contrail climate impact (Burkhardt & Kärcher, 2011; Chen & Gettelman, 2013; Schumann, 2012). This indicates that the fraction of contrail forcing represented by the contrails observed with GEO imagers compared to VIIRS is likely greater than the observation rate of 20% of individual contrails we found. A

quantitative assessment of this metric remains a key aspect of future research. While we point out that GEO imagers might not resolve many young contrails, it should be noted that the comparatively high temporal frequency of GEO observations enables satellite-based assessments of the evolution of individual contrails over time. Future work could leverage this opportunity to provide more temporal context for both the contrails observed and those that were potentially not yet observed with ABI and thereby observationally bound their respective potential radiative impact. This is currently not possible using only LEO imagers due to their long revisit times. Future studies should consider additional image frames and conduct a temporal analysis to capture their evolution to help assess the importance of these omitted contrails and thus further define the implications for identifying regions for navigational avoidance.

Although our results imply limitations in the completeness of GEO observations, there are nuances to how this affects the contrail regions that are derived for deviations. Figure 1a reveals essentially two categories of cases in which contrails are visible with VIIRS but not with ABI. In some instances, ABI omits individual contrails in regions and clusters that are well identified due to neighboring contrail observations (see Inset 1). In other instances, VIIRS reveals additional clusters and regions of contrails that cannot yet, or at least not to their full extent, be identified with geostationary imagers (see Inset 2). Nonetheless, while GEO observations miss 80% of contrails that can be observed with higher-resolution instruments, geostationary satellite data can provide key information on ice-supersaturated regions that is also crucial for real-time navigational contrail avoidance. Missing large numbers of contrails that are observed from other platforms within these regions, therefore, does not necessarily translate to the fraction of accurately identified avoidance regions and consequently does not necessarily limit the success of navigational contrail avoidance approaches to the same degree, as those do not require the identification of all contrails within a certain region, as shown in Inset 1 of Figure 1a.

However, geostationary imagery introduces uncertainty when determining whether or not a certain flight formed a contrail. This also limits the fidelity with which model predictions of humidity can be characterized, which, alongside the identified limitations on assessing avoided contrail lengths, impairs MRV for individual flights. Further, the ABI's lower resolution leads to a misrepresentation of the observed contrails and subsequent overestimates of their widths and cover, up to an average factor of 127%, compounding uncertainty about contrail climate impacts from missed contrail observations and individual contrail appearance. Future assessments should match contrail observations in the respective images of each scene to decompose the effects of resolution limits and missed observations by only considering VIIRS contrails that are also observed with ABI.

Nonetheless, we point out that comparing ABI observations to those from VIIRS does not provide an absolute estimate of how many contrails ABI misses regarding the true population. VIIRS itself is an imperfect imager, which cannot provide observational ground truth on whether contrails are present or absent. Subsequently, it only reveals a fraction of the existing contrails that remain unobserved from ABI. While Kärcher et al. (2009) have inferred from modeling that other polar-orbiting imagers may miss up to half of all contrails, resulting in an underestimate in contrail cover by around 35%, more precise observational ground truth is necessary, yet not available to validate modeling output due to incomplete contrail observations, such as those from GEO imagers, at this time.

Further, we note that our findings are not expected to numerically translate to the statistical output of automated contrail identification methods, which depend on the tuning of the detection parameters to balance the false positive rate against the recall. The detection efficiency of the same method applied to the two data sets might yield less pronounced discrepancies between contrails found in ABI images relative to VIIRS.

While our findings are limited by the number of scenes and the subjective judgment of human labelers, both of which impact the quantitative results we present, they point out important contributors to uncertainties in how much contrails reduce incoming solar radiation and add to longwave warming. However, contrail observations from GEO imagers provide important and continuously sampled information for navigational avoidance. Enhanced by higher-resolution data, the information can be used to evaluate contrail climate models, especially when the fraction of omitted contrail observations and the uncertainty around contrail widths and cover are well understood. The use of observed contrail cover in contrail impact modeling would additionally need to consider a representation of the underlying distribution of contrail optical depths such as the ones presented in Kärcher et al. (2009) and Vázquez-Navarro et al. (2015).

We conclude that contrail observations from geostationary imagers have noteworthy limitations when used on their own for individual evaluations of contrail formation and persistence, as well as for climate impact assessments. Our results highlight the need for increased use of higher-resolution imagers such as those onboard polar-orbiting satellites, as well as ground-based cameras to better resolve individual contrails and complement broadly available GEO data. This will enable us to move toward more refined contrail impact modeling and more rigorous and verifiable avoidance approaches.

Conflict of Interest

The authors declare no conflicts of interest relevant to this study.

Data Availability Statement

The data set, including the investigated satellite images, the contrail binary masks, and all generated contrail labels, alongside their extracted geometric properties, is made publicly available on Zenodo (Euchenhofer et al., 2025).

Acknowledgments
This research was partially funded by the U.S. Federal Aviation Administration Office of Environment and Energy through ASCENT, the FAA Center of Excellence for Alternative Jet Fuels and the Environment, Project 78 through FAA Award Number 13-C-AJFE-MIT under the supervision of Kenisha V. Ford and Nicole Didyk-Wells. Any opinions, findings, conclusions or recommendations expressed in this material are those of the authors and do not necessarily reflect the views of the FAA. The authors thank two anonymous reviewers for their constructive comments that improved this manuscript.

References

Agarwal, A., Meijer, V. R., Eastham, S. D., Speth, R. L., & Barrett, S. R. (2022). Reanalysis-driven simulations may overestimate persistent contrail formation by 100%–250%. *Environmental Research Letters*, *17*(1), 014045. https://doi.org/10.1088/1748-9326/ac38d9

Appleman, H. (1953). The formation of exhaust condensation trails by jet aircraft. *Bulletin of the American Meteorological Society*, *34*(1), 14–20. https://doi.org/10.1175/1520-0477-34.1.14

Bakan, S., Betancor, M., Gayler, V., & Graßl, H. (1994). Contrail frequency over Europe from NOAA satellite images. *Annales Geophysicae*, *12*(10/11), 962–968. https://doi.org/10.1007/s00585-994-0962-y

Bedka, S. T., Minnis, P., Duda, D. P., Chee, T. L., & Palikonda, R. (2013). Properties of linear contrails in the Northern Hemisphere derived from 2006 Aqua MODIS observations. *Geophysical Research Letters*, *40*(4), 772–777. https://doi.org/10.1029/2012GL054363

Bier, A., & Burkhardt, U. (2022). Impact of parametrizing microphysical processes in the jet and vortex phase on contrail cirrus properties and radiative forcing. *Journal of Geophysical Research: Atmospheres*, *127*(23), e2022JD036677. https://doi.org/10.1029/2022jd036677

Bock, L., & Burkhardt, U. (2016). Reassessing properties and radiative forcing of contrail cirrus using a climate model. *Journal of Geophysical Research: Atmospheres*, *121*(16), 9717–9736. https://doi.org/10.1002/2016jd025112

Burkhardt, U., & Kärcher, B. (2011). Global radiative forcing from contrail cirrus. *Nature Climate Change*, *1*(1), 54–58. https://doi.org/10.1038/nclimate1068

Burkhardt, U., Kärcher, B., & Schumann, U. (2010). Global modeling of the contrail and contrail cirrus climate impact. *Bulletin of the American Meteorological Society*, *91*(4), 479–484. https://doi.org/10.1175/2009bams2656.1

Chen, C.-C., & Gettelman, A. (2013). Simulated radiative forcing from contrails and contrail cirrus. *Atmospheric Chemistry and Physics*, *13*(24), 12525–12536. https://doi.org/10.5194/acp-13-12525-2013

Chevallier, R., Shapiro, M., Engberg, Z., Soler, M., & Delahaye, D. (2023). Linear contrails detection, tracking and matching with aircraft using geostationary satellite and air traffic data. *Aerospace*, *10*(7), 578. https://doi.org/10.3390/aerospace10070578

Driver, O. G. A., Stettler, M. E. J., & Gryspeerdt, E. (2024). *Factors limiting contrail detection in satellite imagery* (pp. 1–28). EGUsphere. https://doi.org/10.5194/egusphere-2024-2198

Duda, D. P., Bedka, S. T., Minnis, P., Spangenberg, D., Khlopenkov, K., Chee, T., & Smith, W. L., Jr. (2019). Northern Hemisphere contrail properties derived from Terra and Aqua MODIS data for 2006 and 2012. *Atmospheric Chemistry and Physics*, *19*(8), 5313–5330. https://doi.org/10.5194/acp-19-5313-2019

Duda, D. P., Minnis, P., Khlopenkov, K., Chee, T. L., & Boeke, R. (2013). Estimation of 2006 Northern Hemisphere contrail coverage using MODIS data. *Geophysical Research Letters*, *40*(3), 612–617. https://doi.org/10.1002/grl.50097

Duda, D. P., Minnis, P., Nguyen, L., & Palikonda, R. (2004). A case study of the development of contrail clusters over the great lakes. *Journal of the Atmospheric Sciences*, *61*(10), 1132–1146. https://doi.org/10.1175/1520-0469(2004)061<1132:acsotd>2.0.co;2

Euchenhofer, M. V., Prashanth, P., Parke, S. A., Eastham, S. D., & Waitz, I. A. (2025). Dataset of manually identified contrails in goes abi and viirs satellite imagery [Dataset]. *Zenodo*. https://doi.org/10.5281/zenodo.16332566

Geraedts, S., Brand, E., Dean, T. R., Eastham, S., Elkin, C., Engberg, Z., et al. (2024). A scalable system to measure contrail formation on a per-flight basis. *Environmental Research Communications*, *6*(1), 015008. https://doi.org/10.1088/2515-7620/ad11ab

Gierens, K., Matthes, S., & Rohs, S. (2020). How well can persistent contrails be predicted? *Aerospace*, *7*(12), 169. https://doi.org/10.3390/aerospace7120169

Gierens, K., & Vázquez-Navarro, M. (2018). Statistical analysis of contrail lifetimes from a satellite perspective. *Meteorologische Zeitschrift*, 183–193. https://doi.org/10.1127/metz/2018/0888

Haywood, J. M., Allan, R. P., Bornemann, J., Forster, P. M., Francis, P. N., Milton, S., et al. (2009). A case study of the radiative forcing of persistent contrails evolving into contrail-induced cirrus. *Journal of Geophysical Research*, *114*(D24), D24201. https://doi.org/10.1029/2009jd012650

Jensen, E. J., Toon, O. B., Kinne, S., Sachse, G. W., Anderson, B. E., Chan, K. R., et al. (1998). Environmental conditions required for contrail formation and persistence. *Journal of Geophysical Research*, *103*(D4), 3929–3936. https://doi.org/10.1029/97jd02808

Kärcher, B. (2018). Formation and radiative forcing of contrail cirrus. *Nature Communications*, *9*(1), 1824. https://doi.org/10.1038/s41467-018-04068-0

Kärcher, B., Burkhardt, U., Bier, A., Bock, L., & Ford, I. J. (2015). The microphysical pathway to contrail formation. *Journal of Geophysical Research: Atmospheres*, *120*(15), 7893–7927. https://doi.org/10.1002/2015JD023491

Kärcher, B., Burkhardt, U., Unterstrasser, S., & Minnis, P. (2009). Factors controlling contrail cirrus optical depth. *Atmospheric Chemistry and Physics*, *9*(16), 6229–6254. https://doi.org/10.5194/acp-9-6229-2009

Kulik, L. (2019). *Satellite-based detection of contrails using deep learning (thesis)*. Massachusetts Institute of Technology.
Lee, D. S., Fahey, D. W., Skowron, A., Allen, M. R., Burkhardt, U., Chen, Q., et al. (2021). The contribution of global aviation to anthropogenic climate forcing for 2000 to 2018. *Atmospheric Environment*, *244*, 117834. https://doi.org/10.1016/j.atmosenv.2020.117834
Low, J., Teoh, R., Ponsonby, J., Gryspeerdt, E., Shapiro, M., & Stettler, M. E. (2025). Ground-based contrail observations: Comparisons with reanalysis weather data and contrail model simulations. *Atmospheric Measurement Techniques*, *18*(1), 37–56. https://doi.org/10.5194/amt-18-37-2025
Mannstein, H., Brömser, A., & Bugliaro, L. (2010). Ground-based observations for the validation of contrails and cirrus detection in satellite imagery. *Atmospheric Measurement Techniques*, *3*(3), 655–669. https://doi.org/10.5194/amt-3-655-2010
Mannstein, H., Meyer, R., & Wendling, P. (1999). Operational detection of contrails from NOAA-AVHRR-data. *International Journal of Remote Sensing*, *20*(8), 1641–1660. https://doi.org/10.1080/014311699212650
Marquart, S., Ponater, M., Mager, F., & Sausen, R. (2003). Future development of contrails: Impacts of increasing air traffic and climate change. In *Paper presented at the proceedings of the AAC-conference*. June 30 to July 3, 2003, Friedrichshafen, Germany.
Meerkötter, R., Schumann, U., Doelling, D. R., Minnis, P., Nakajima, T., & Tsushima, Y. (1999). Radiative forcing by contrails. *Annales Geophysicae*, *17*(8), 1080–1094. https://doi.org/10.1007/s00585-999-1080-7
Meijer, V. R. (2024). *Satellite-based analysis and forecast evaluation of aviation contrails*. (PhD Thesis). Massachusetts Institute of Technology.
Meijer, V. R., Kulik, L., Eastham, S. D., Allroggen, F., Speth, R. L., Karaman, S., & Barrett, S. R. H. (2022). Contrail coverage over the United States before and during the COVID-19 pandemic. *Environmental Research Letters*, *17*(3), 034039. https://doi.org/10.1088/1748-9326/ac26f0
Meyer, R., Mannstein, H., Meerkötter, R., Schumann, U., & Wendling, P. (2002). Regional radiative forcing by line-shaped contrails derived from satellite data. *Journal of Geophysical Research*, *107*(D10), ACL–17. https://doi.org/10.1029/2001jd000426
Minnis, P., Ayers, J. K., Nordeen, M. L., & Weaver, S. P. (2003). Contrail frequency over the United States from surface observations. *Journal of Climate*, *16*(21), 3447–3462. https://doi.org/10.1175/1520-0442(2003)016⟨3447:CFOTUS⟩2.0.CO;2
Minnis, P., Ayers, J. K., & Weaver, S. P. (1997). *Surface-based observations of contrail occurrence frequency over the US, April 1993–April 1994* (Vol. 1404, pp. 1157–1160). NASA Reference Publication.
Minnis, P., Bedka, S. T., Duda, D. P., Bedka, K. M., Chee, T., Ayers, J. K., et al. (2013). Linear contrail and contrail cirrus properties determined from satellite data. *Geophysical Research Letters*, *40*(12), 3220–3226. https://doi.org/10.1002/grl.50569
Minnis, P., Palikonda, R., Walter, B. J., Ayers, J. K., & Mannstein, H. (2005). Contrail properties over the eastern north Pacific from avhrr data. *Meteorologische Zeitschrift*, *14*(4), 515–524. https://doi.org/10.1127/0941-2948/2005/0056
Minnis, P., Trepte, Q. Z., Sun-Mack, S., Chen, Y., Doelling, D. R., Young, D. F., et al. (2008). Cloud detection in nonpolar regions for CERES using TRMM VIRS and terra and aqua MODIS data. *IEEE Transactions on Geoscience and Remote Sensing*, *46*(11), 3857–3884. https://doi.org/10.1109/TGRS.2008.2001351
Ng, J. Y.-H., McCloskey, K., Cui, J., Meijer, V. R., Brand, E., Sarna, A., et al. (2023). Contrail detection on GOES-16 ABI with the OpenContrails dataset. *IEEE Transactions on Geoscience and Remote Sensing*, *62*, 1–14. https://doi.org/10.1109/TGRS.2023.3345226
Palikonda, R., Minnis, P., Duda, D. P., & Mannstein, H. (2005). Contrail coverage derived from 2001 AVHRR data over the continental United States of America and surrounding areas. *Meteorologische Zeitschrift*, *14*(4), 525–536. https://doi.org/10.1127/0941-2948/2005/0051
Sanz-Morère, I., Eastham, S. D., Speth, R. L., & Barrett, S. R. (2020). Reducing uncertainty in contrail radiative forcing resulting from uncertainty in ice crystal properties. *Environmental Science and Technology Letters*, *7*(6), 371–375. https://doi.org/10.1021/acs.estlett.0c00150
Schumann, U. (1996). On conditions for contrail formation from aircraft exhausts. *Meteorologische Zeitschrift*, *5*(1), 4–23. https://doi.org/10.1127/metz/5/1996/4
Schumann, U. (2012). A contrail cirrus prediction model. *Geoscientific Model Development*, *5*(3), 543–580. https://doi.org/10.5194/gmd-5-543-2012
Schumann, U., Hempel, R., Flentje, H., Garhammer, M., Graf, K., Kox, S., et al. (2013). Contrail study with ground-based cameras. *Atmospheric Measurement Techniques*, *6*(12), 3597–3612. https://doi.org/10.5194/amt-6-3597-2013
Shenk, W. E., & Salomonson, V. V. (1972). A simulation study exploring the effects of sensor spatial resolution on estimates of cloud cover from satellites. *Journal of Applied Meteorology and Climatology*, *11*(1), 214–220. https://doi.org/10.1175/1520-0450(1972)011⟨0214:ASSETE⟩2.0.CO;2
Sonabend-W, A., Elkin, C., Dean, T., Dudley, J., Ali, N., Blickstein, J., et al. (2024). Feasibility test of per-flight contrail avoidance in commercial aviation. *Communications Engineering*, *3*(1), 184. https://doi.org/10.1038/s44172-024-00329-7
Teoh, R., Engberg, Z., Schumann, U., Voigt, C., Shapiro, M., Rohs, S., & Stettler, M. E. (2024). Global aviation contrail climate effects from 2019 to 2021. *Atmospheric Chemistry and Physics*, *24*(10), 6071–6093. https://doi.org/10.5194/acp-24-6071-2024
Teoh, R., Schumann, U., Majumdar, A., & Stettler, M. E. (2020). Mitigating the climate forcing of aircraft contrails by small-scale diversions and technology adoption. *Environmental Science & Technology*, *54*(5), 2941–2950. https://doi.org/10.1021/acs.est.9b05608
Vázquez-Navarro, M., Mannstein, H., & Kox, S. (2015). Contrail life cycle and properties from 1 year of MSG/SEVIRI rapid-scan images. *Atmospheric Chemistry and Physics*, *15*(15), 8739–8749. https://doi.org/10.5194/acp-15-8739-2015
Vazquez-Navarro, M., Mannstein, H., & Mayer, B. (2010). An automatic contrail tracking algorithm. *Atmospheric Measurement Techniques*, *3*(4), 1089–1101. https://doi.org/10.5194/amt-3-1089-2010
Wang, Z., Bugliaro, L., Jurkat-Witschas, T., Heller, R., Burkhardt, U., Ziereis, H., et al. (2022). Observations of microphysical properties and radiative effects of contrail cirrus and natural cirrus over the north Atlantic. *Atmospheric Chemistry and Physics Discussions*, 1–36.